

# TWO-LEVEL OVERLAPPING ADDITIVE SCHWARZ PRECONDITIONER FOR TRAINING SCIENTIFIC MACHINE LEARNING APPLICATIONS \*

YOUNGKYU LEE<sup>†</sup>, ALENA KOPANIČÁKOVÁ<sup>†‡</sup>, AND GEORGE EM KARNIADAKIS<sup>†§</sup>

**Abstract.** We introduce a novel two-level overlapping additive Schwarz preconditioner for accelerating the training of scientific machine learning applications. The design of the proposed preconditioner is motivated by the nonlinear two-level overlapping additive Schwarz preconditioner. The neural network parameters are decomposed into groups (subdomains) with overlapping regions. In addition, the network’s feed-forward structure is indirectly imposed through a novel subdomain-wise synchronization strategy and a coarse-level training step. Through a series of numerical experiments, which consider physics-informed neural networks and operator learning approaches, we demonstrate that the proposed two-level preconditioner significantly speeds up the convergence of the standard (LBFGS) optimizer while also yielding more accurate machine learning models. Moreover, the devised preconditioner is designed to take advantage of model-parallel computations, which can further reduce the training time.

**Key words.** scientific machine learning, nonlinear preconditioning, Schwarz methods, domain-decomposition

**MSC codes.** 90C30, 90C26, 90C06, 65M55, 68T07

**1. Introduction.** Deep neural networks (DNNs) are universal approximators, capable of approximating any continuous function defined on a compact domain to arbitrary accuracy [4, 11, 62]. Therefore, they have been recently widely used to obtain ansatz spaces for the solutions of partial differential equations (PDEs) for a wide range of scientific and engineering problems; see [35] for an overview. The popularity of these DNN approaches can be largely attributed to their simplicity, mesh-free nature, and ability to incorporate data [60, 63], enabling them to effectively tackle complex, high-dimensional, forward and inverse problems in single and multi-query scenarios [56].

Two prominent approaches for solving parametric PDEs using DNNs appear in the literature. The first approach approximates a solution of a given PDE for a particular choice of parameters using a DNN [60, 63]. Popular representatives of this approach are physics informed neural networks (PINNs) [60], which train the DNNs by minimizing the mean square error that incorporates the PDE residual, boundary/initial conditions, and/or observed data. The second approach considers learning the differential operator [52, 67] from the parametrized source terms, boundary/initial conditions, or material properties. The operator learning DNNs, such as DeepONet (DON) [52] or FNO [49], are typically trained by minimizing the mean square error

---

\*Submitted to the editors 30-June-2024.

**Funding:** Y.L. was supported in part by Basic Science Research Program through NRF funded by the Ministry of Education (No. RS2023-00247199). A.K. was supported by the Swiss National Science Foundation (SNSF) under the projects “*Multilevel training of DeepONets – multiscale and multiphysics applications*” and “*ML<sup>2</sup> - Multilevel and Domain Decomposition Methods for Machine Learning*”, as well as by the Platform for Advanced Scientific Computing (PASC) under the project *ExaTrain*. G.E.K. is supported by the ONR Vannevar Bush Faculty Fellowship. We also acknowledge support from the DOE-MMICS SEA-CROGS DE-SC0023191 award and Ansys Inc.

<sup>†</sup>Division of Applied Mathematics, Brown University, Providence, USA ([youngkyu\\_lee@brown.edu](mailto:youngkyu_lee@brown.edu), [alena\\_kopanicakova@brown.edu](mailto:alena_kopanicakova@brown.edu), [george\\_karniadakis@brown.edu](mailto:george_karniadakis@brown.edu)).

<sup>‡</sup>Euler Institute, Università della Svizzera italiana, Lugano, Switzerland ([alena.kopanicakova@usi.ch](mailto:alena.kopanicakova@usi.ch)).

<sup>§</sup>School of Engineering, Brown University, Providence, USA

between the network’s output and the solution generated using a high-fidelity method.

Both, the physics informed and operator learning, approaches are commonly trained using gradient-based optimizers, e.g., Adam [36] or LBFGS [51]. However, the computational cost of these optimizers can be exorbitant due to the non-convexity and ill-conditioning of the underlying optimization problem. This is especially the case when a highly accurate solution is required. In order to reduce the training time, the parallelization of the DNN training process has gained significant attention in the literature; see, for example [5, 13]. Two of the most popular parallel paradigms are data-parallel and model-parallel approaches. Data-parallel approaches [45] split the training data among multiple processing devices. Each device then evaluates the loss/gradient for a given portion of data, and the average value is used to update the network parameters. In contrast, model-parallel approaches aim at splitting the parameters of the DNN model among multiple devices, see for example pipelining techniques [30, 58] or tensor-parallel approaches [5, 61].

In numerical analysis, domain decomposition (DD) methods are commonly used to accelerate the convergence and parallelize solution strategies for large-scale problems [18, 65]. Among these approaches, the additive Schwarz method (ASM) [50] is widely utilized for its simplicity and parallel computing capabilities. In ASM, the computational domain is first decomposed into a collection of smaller, possibly overlapping, subdomains. The solution of a PDE is then sought in parallel for each subdomain, and the acquired local solutions are subsequently combined to update the global solution approximation.

Although the ASM is parallelizable by design, it is not algorithmically scalable, as its convergence tends to deteriorate with an increased number of subdomains [18, 65]. The common remedy for achieving the algorithmic scalability, i.e., keeping the number of iterations bounded independently of the number of subdomains, is to introduce: i) overlap between the subdomains ii) a coarse-level correction step, giving rise to the two-level overlapping additive Schwarz method (TL-ASM) [19]. The role of the overlap is to provide the continuity between local solutions at the interface, while the coarse-level correction step ensures the transfer of data across the entire domain at marginal computational cost [20]. Building upon these advancements, our goal is to construct the nonlinear TL-ASM in order to parallelize the training of scientific machine learning applications while at the same time enhancing the convergence speed of the current state-of-the-art optimizers.

In the field of machine learning, DD approaches are increasingly utilized to enhance the training of DNNs. For example, the parallelization of training through the decomposition of deep convolutional networks has been proposed in [25, 37]. In [26, 40, 47], multilevel decompositions giving rise to layer-parallel training have been explored. Moreover, in the context of PINNs, several DD-based approaches that leverage the spatiotemporal decomposition of the computational domain have been proposed, such as XPINN [32], cPINN [34], APINN [29], and multilevel DD-based architectures [16, 48]. In this work, we build upon the recent work presented in [40], where single-level additive and multiplicative preconditioners for training of PINNs were introduced. These preconditioners utilize the layer-wise decomposition of DNNs and are, therefore, agnostic to the underlying physics and computational domain. This suggests their potential use beyond the training of PINNs to a broader range of scientific machine learning problems, including data-driven operator learning approaches.

Starting from the single-level additive layer-wise preconditioner [40], we devise a novel two-level overlapping additive Schwarz preconditioner by leveraging and ex-

panding established techniques from numerical analysis related to nonlinear two-level additive Schwarz methods (TL-ASM) [9, 15, 41, 44, 55]. The main contributions of this work can be summarized as follows.

- We introduce overlapping layer-wise decomposition of DNNs, effectively improving the convergence of non-overlapping layer-wise preconditioners.
- A novel subdomain-wise synchronization strategy is proposed to recombine corrections obtained from parallel subdomain training. This expands upon commonly used methodologies in numerical analysis, which combine subdomain corrections using the weighted averaging technique, see for example literature on the (nonlinear) restricted ASM [9, 10].
- We incorporate a coarse-level training step, which enables the global communication between subdomains while maintaining the feed-forward nature of feature flow in the DNNs.
- The applicability of the single-level and eventually two-level layer-wise preconditioners is extended beyond PINNs to DeepONets.
- Through numerical experiments, we demonstrate that the proposed two-level preconditioner yields more accurate DNN models, while also improving the convergence rate of the standard LBFGS optimizer and the baseline single-level preconditioner [40].

This paper is organized as follows. Section 2 provides an introduction to scientific machine learning, with a particular focus on PINNs and DeepONets. In Section 3, we propose a novel two-level overlapping additive Schwarz preconditioner for training DNNs. Section 4 presents a set of benchmark problems and discusses the implementation details. Finally, in Section 5, we demonstrate the numerical performance of the proposed preconditioner. The conclusion and future work are discussed in Section 6.

**2. Scientific machine learning.** Scientific machine learning is an emerging research field that integrates scientific computing with machine learning techniques to solve complex scientific and engineering problems. In this work, we focus our attention on solving the parameterized PDEs using PINNs [60] and DONs [52]. To this aim, let  $\Omega \subset \mathbb{R}^d$ ,  $d = 1, 2$ , or  $3$ , be a closed bounded domain and let the parameter set  $\mathbf{H}$  be a compact subset of  $\mathbb{R}^p$ , where  $p \geq 0$ . The parametric PDE is given in its abstract form as: For  $\boldsymbol{\eta} \in \mathbf{H}$ , find  $u(\mathbf{x}, \boldsymbol{\eta}): \Omega \times \mathbf{H} \rightarrow \mathbb{R}$ , such that

$$(2.1) \quad \begin{aligned} \mathcal{A}(u(\mathbf{x}, \boldsymbol{\eta}), \boldsymbol{\eta}) &= f(\mathbf{x}, \boldsymbol{\eta}), & \mathbf{x} \in \Omega, \\ \mathcal{B}^k(u(\mathbf{x}, \boldsymbol{\eta}), \boldsymbol{\eta}) &= g^k(\mathbf{x}, \boldsymbol{\eta}), & \mathbf{x} \in \Gamma^k \subseteq \partial\Omega, \quad \text{for } k = 1, 2, \dots, n_\Gamma, \end{aligned}$$

where  $\mathcal{A}$  and  $\{\mathcal{B}\}_{k=1}^{n_\Gamma}$  denote a nonlinear differential operator and a set of boundary condition operators<sup>1</sup>, respectively. Moreover, the right hand side function  $f(\mathbf{x}, \boldsymbol{\eta})$  and the functions  $\{g^k(\mathbf{x}, \boldsymbol{\eta})\}_{k=1}^{n_\Gamma}$  are given.

**2.1. Physics informed neural networks.** PINNs [60] leverage empirical data and knowledge of physical priors to solve PDEs using DNNs. Here, we focus on solving one particular instance of (2.1) with a preselected set of parameters  $\boldsymbol{\eta}$ . A solution  $u(\mathbf{x}, \boldsymbol{\eta})$  of a PDE for a given  $\boldsymbol{\eta}$  at any  $\mathbf{x} \in \Omega$  is approximated by the DNN  $u_\boldsymbol{\theta}: \mathbb{R}^d \rightarrow \mathbb{R}$ , which is parameterized with respect to parameters  $\boldsymbol{\theta} \in \mathbb{R}^n$ . An actual form of the DNN depends on the user-specified neural network architecture. For instance,  $u_\boldsymbol{\theta}$  can be represented by a feed-forward network or a residual network [28].

<sup>1</sup>In the case of time-dependent problems, we handle the time dimension as an additional component of the vector  $\mathbf{x} \in \Omega$ , which allows us to treat the initial condition as a specific type of the boundary conditions.

In order to ensure that the network  $u_{\boldsymbol{\theta}}$  approximates the PDE, we have to find the optimal set of DNN's parameters  $\boldsymbol{\theta}^*$ . To this aim, we minimize the loss  $\mathcal{L}: \mathbb{R}^n \rightarrow \mathbb{R}$  associated with a residual of a given PDE and boundary conditions, i.e.,

$$(2.2) \quad \boldsymbol{\theta}^* = \arg \min_{\boldsymbol{\theta} \in \mathbb{R}^n} \mathcal{L}(\boldsymbol{\theta}) := w_{\text{int}} \mathcal{L}_{\text{int}}(\boldsymbol{\theta}) + w_{\text{bc}} \mathcal{L}_{\text{bc}}(\boldsymbol{\theta}),$$

where

$$(2.3) \quad \begin{aligned} \mathcal{L}_{\text{int}}(\boldsymbol{\theta}) &:= \|\mathcal{A}(u_{\boldsymbol{\theta}}) - f\|_{L^2(\Omega)}^2 = \int_{\Omega} (\mathcal{A}(u_{\boldsymbol{\theta}}(\mathbf{x})) - f(\mathbf{x}))^2 d\mathbf{x}, \\ \mathcal{L}_{\text{bc}}(\boldsymbol{\theta}) &:= \|\mathcal{B}(u_{\boldsymbol{\theta}}) - g\|_{L^2(\partial\Omega)}^2 = \int_{\partial\Omega} (\mathcal{B}(u_{\boldsymbol{\theta}}(\mathbf{x})) - g(\mathbf{x}))^2 d\mathbf{x}. \end{aligned}$$

To discretize the interior loss  $\mathcal{L}_{\text{int}}$ , we consider a set of points  $\mathcal{D}_{\text{int}} = \{\mathbf{x}_j\}_{j=1}^{n_{\text{int}}}$  sampled from the interior of the domain  $\Omega$ . Similarly, in order to discretize the boundary loss  $\mathcal{L}_{\text{bc}}$ , we construct  $\{\mathcal{D}_{\text{bc}}^k\}_{k=1}^{n_{\Gamma}}$ , where each point of  $\mathcal{D}_{\text{bc}}^k = \{\mathbf{x}_j^k\}_{j=1}^{n_{\text{bc}}^k}$  is sampled from the boundary  $\Gamma^k$ . The continuous losses (2.3) can be then discretized, for example, by using the Monte-Carlo method, giving rise to

$$\begin{aligned} \mathcal{L}_{\text{int}}(\boldsymbol{\theta}) &= \frac{1}{|\mathcal{D}_{\text{int}}|} \sum_{\mathbf{x}_j \in \mathcal{D}_{\text{int}}} (\mathcal{A}(u_{\boldsymbol{\theta}}(\mathbf{x}_j)) - f(\mathbf{x}_j))^2, \\ \mathcal{L}_{\text{bc}}(\boldsymbol{\theta}) &= \sum_{k=1}^{n_{\Gamma}} \left( \frac{1}{|\mathcal{D}_{\text{bc}}^k|} \sum_{\mathbf{x}_j^k \in \mathcal{D}_{\text{bc}}^k} (\mathcal{B}(u_{\boldsymbol{\theta}}(\mathbf{x}_j^k)) - g(\mathbf{x}_j^k))^2 \right). \end{aligned}$$

The weights  $w_{\text{int}}$  and  $w_{\text{bc}}$  in (2.2) are used to balance the interior and boundary loss terms. In practice, the quality of the DNN approximation and the success of the training process depends on the appropriate selection of these weights [64]. Consequently, many approaches for manual or automatic selection of weights have been proposed in the literature; see, for instance, NTK-based weighting strategies [68] or residual-based attention mechanism [1]. In this work, we opt to avoid selecting  $w_{\text{int}}, w_{\text{bc}}$  by directly incorporating the boundary conditions into the network architecture. Following [54, 64], we modify the network output as

$$(2.4) \quad \tilde{u}_{\boldsymbol{\theta}}(\mathbf{x}) := \sum_{k=1}^{n_{\Gamma}} g^k(\mathbf{x}) + \ell(\mathbf{x}) u_{\boldsymbol{\theta}}(\mathbf{x}), \quad \text{where } \ell(\mathbf{x}) := \prod_{k=1}^{n_{\Gamma}} (1 - (1 - \ell^k(\mathbf{x}))).$$

Each function  $\ell^k: \Omega \rightarrow [0, 1]$  is defined such that

$$\ell^k(\mathbf{x}) = \begin{cases} 0, & \mathbf{x} \in \Gamma^k, \\ 1, & \mathbf{x} \in \Gamma^j, \quad j \in \{1, 2, \dots, n_{\Gamma}\}, \quad \text{for } k \neq j, \\ t \in (0, 1), & \text{otherwise.} \end{cases}$$

Using  $\tilde{u}_{\boldsymbol{\theta}}$  as defined in (2.4), we can now reformulate the minimization problem (2.2) as

$$(2.5) \quad \boldsymbol{\theta}^* = \arg \min_{\boldsymbol{\theta} \in \mathbb{R}^n} \mathcal{L}(\boldsymbol{\theta}) := \frac{1}{|\mathcal{D}_{\text{int}}|} \sum_{\mathbf{x}_j \in \mathcal{D}_{\text{int}}} (\mathcal{A}(\tilde{u}_{\boldsymbol{\theta}}(\mathbf{x}_j)) - f(\mathbf{x}_j))^2.$$

**2.2. Operator learning.** Operator learning approaches use DNNs to approximate a mapping between infinite-dimensional function spaces. Let  $\mathcal{Y}$  be an infinite-dimensional Banach space, which can represent a space of parametrized right-hand sides, boundary conditions, or material parameters. The goal is to approximate the operator  $\mathcal{G}: \mathcal{Y} \rightarrow \mathcal{V}$ , where  $\mathcal{V}$  denotes the solution space of the parametric PDE, specified by (2.1). In this work, we approximate the operator  $\mathcal{G}$  using the DON, initially proposed in [52].

The architecture of DON consists of branch and trunk networks. The branch network  $B: \mathcal{Y}_m \rightarrow \mathbb{R}^p$  provides a set of  $p$  coefficients for a given discretized function  $\mathbf{y} \in \mathcal{Y}_m$ . Here,  $\mathcal{Y}_m$  is a  $m$ -dimensional space that is assumed to satisfy the following condition:

$$\forall \mathbf{y} \in \mathcal{Y}, \exists \mathbf{y}_m \in \mathcal{Y}_m \text{ such that } \mathbf{y}_m \rightarrow \mathbf{y} \text{ as } m \rightarrow \infty.$$

In addition, the trunk network  $T: \Omega \rightarrow \mathbb{R}^p$  is used to encode the computational domain  $\Omega$ . Therefore, it takes as an input a coordinate  $\boldsymbol{\xi} \in \Omega$  and returns a set of  $p$  basis functions.

The coefficients  $B_k(\mathbf{y}) \in \mathbb{R}^p$  and the basis functions  $T_k(\boldsymbol{\xi}) \in \mathbb{R}^p$  obtained as an output of branch and trunk networks are then combined as

$$(2.6) \quad \mathcal{G}_\theta(\mathbf{y})(\boldsymbol{\xi}) := \sum_{k=1}^p B_k(\mathbf{y})T_k(\boldsymbol{\xi}), \quad \mathbf{y} \in \mathcal{Y}_m, \boldsymbol{\xi} \in \Omega,$$

to approximate a solution of the parametric PDE at a point  $\boldsymbol{\xi}$  for a given function  $\mathbf{y}$ . Figure 2.1 illustrates a prototypical DON architecture. Note that we are free to choose the architecture of branch and trunk networks. For example, the choice of the branch network can be guided by the structure of the input  $\mathbf{y}$ , e.g., it can be a fully connected network in case of a scalar inputs, or a convolutional network in case of multidimensional discretized functions. Since the vector of coordinates  $\boldsymbol{\xi} \in \mathbb{R}^d$  is usually low dimensional, fully connected networks are commonly used in place of the trunk network. Alternatively, one can utilize the precomputed basis functions, e.g., obtained by means of the proper orthogonal decomposition (POD) performed on the training data [53] or by means of parameterizing the integral kernel in the Fourier space [2].

To train DON such that it approximates solutions of (2.1), we construct a dataset

$$\mathcal{D} = \{(\mathbf{y}_j, \bar{\boldsymbol{\xi}}_j, \mathbf{u}_j)\}_{j=1}^{n_s},$$

consisting of  $n_s$  samples. Each triple  $(\mathbf{y}_j, \bar{\boldsymbol{\xi}}_j, \mathbf{u}_j)$  consists of the discretized function  $\mathbf{y}_j \in \mathbb{R}^m$ , sampled from  $\mathcal{Y}_m$ . Moreover,  $\bar{\boldsymbol{\xi}}_j = [\boldsymbol{\xi}_{j,1}, \dots, \boldsymbol{\xi}_{j,n_c}]^T \in \mathbb{R}^{n_c \times d}$  represents a set of  $n_c$  collocation points and  $\mathbf{u}_j \in \mathbb{R}^{n_c}$  is a target solution evaluated at collocation points constituting  $\bar{\boldsymbol{\xi}}_j$ .

Using dataset  $\mathcal{D}$ , the optimal parameters of the DON, denoted by  $\boldsymbol{\theta}^* \in \mathbb{R}^n$ , are found by solving the following minimization problem:

$$(2.7) \quad \boldsymbol{\theta}^* = \arg \min_{\boldsymbol{\theta} \in \mathbb{R}^n} \mathcal{L}(\boldsymbol{\theta}) := \frac{1}{n_s n_c} \sum_{j=1}^{n_s} \sum_{t=1}^{n_c} (\mathcal{G}_\theta(\mathbf{y}_j)(\boldsymbol{\xi}_{j,t}) - \mathbf{u}_j)^2.$$

Note that instead of using  $\mathbf{u}_j$  given by the dataset, we can utilize the PINN-based loss function; see [67] for details. This might simplify the generation of the dataset

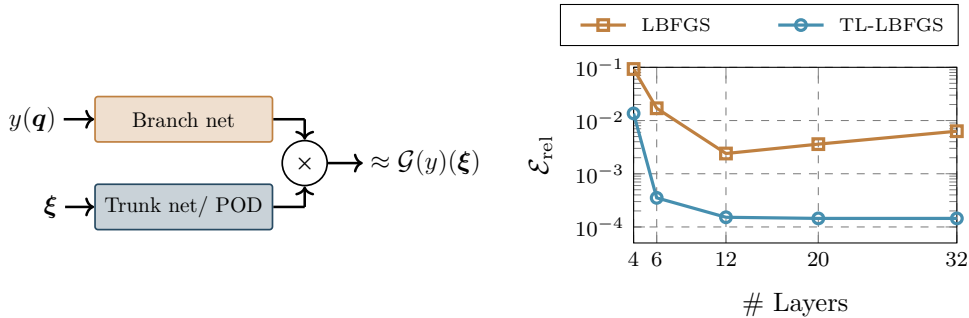


Fig. 2.1: Left: A sketch of DON architecture. The trunk can be represented by the DNN or by the POD basis obtained from the training data. The symbol  $\times$  denotes the inner product between the output of the branch and trunk networks. Right: A relative error obtained by using the standard LBFGS optimizer and the proposed TL-LBFGS as a function of increasing number of layers. The experiment is performed for the AC example, specified in Section 4.1.

but makes the training process more tedious. We do not pursue this possibility here but rather investigate the performance of the proposed two-level preconditioners in data-driven settings. Notably, the proposed preconditioner is expected to enhance the performance of standard optimizers more significantly in the case of PINN-based loss due to increased ill-conditioning of the training problem [67].

**3. Two-level overlapping additive Schwarz preconditioner.** In this work, we focus on training the DNN by solving the following minimization problem:

$$(3.1) \quad \min_{\theta} \mathcal{L}(\theta),$$

where the loss  $\mathcal{L}$  is as defined in (2.5) or (2.7) for PINN or DON, respectively. The minimization problem (3.1) is traditionally solved using gradient-based optimizers such as Adam [36] or LBFGS [51]. However, the convergence of these optimizers tends to deteriorate as problem stiffness and ill-conditioning increase [66], resulting in slow training and unsatisfactory accuracy of the resulting PINN/DON models. For instance, Figure 2.1 illustrates how increasing the number of layers in a PINN model exacerbates the ill-conditioning and non-convexity of the underlying minimization problem. This, in turn, presents significant challenges for the standard LBFGS method to converge, leading to poorer accuracy of the PINN as the representation capacity of the DNN increases.

To overcome these difficulties, the single-level Schwarz preconditioning strategy, which utilizes the layer-wise decomposition of the DNN, was introduced in [40]. In this work, we propose enhancing the performance of this strategy by introducing overlap, a coarse-level correction step, and a subdomain-based recombination strategy. The culmination of these techniques results in a novel two-level overlapping Schwarz preconditioner, the performance of which does not deteriorate with increasing network depth, as shown in Figure 2.1.

To present the proposed two-level overlapping Schwarz preconditioning strategy, let us consider the nonlinear systems of equations associated with the first-order op-

tinality conditions of (3.1) given as

$$(3.2) \quad \nabla \mathcal{L}(\boldsymbol{\theta}) = 0.$$

Since solving (3.2) is computationally demanding, we instead construct and solve the following nonlinearly-preconditioned system of equations:

$$(3.3) \quad \mathcal{F}(\boldsymbol{\theta}) := \nabla \mathcal{L}(\mathcal{M}(\boldsymbol{\theta})) = 0,$$

where the preconditioner  $\mathcal{M}: \mathbb{R}^n \rightarrow \mathbb{R}^n$  is designed such that (3.3) has more balanced nonlinearities than (3.2).

In this work, we solve the nonlinear system (3.3) iteratively. Thus, on each  $k$ -th iteration, we start from a given iterate  $\boldsymbol{\theta}^{(k)}$ , and apply the preconditioner  $\mathcal{M}$ . As a result, we obtain the smoothed iterate  $\boldsymbol{\theta}^{(k+1/2)} := \mathcal{M}(\boldsymbol{\theta}^{(k)})$ , which is required to reduce the loss, i.e., it has to satisfy the following condition:

$$\mathcal{L}(\boldsymbol{\theta}^{(k+1/2)}) \leq \mathcal{L}(\boldsymbol{\theta}^{(k)}).$$

The smoothing step is followed by a global optimization step. To this aim, we apply an operator  $\mathcal{K}: \mathbb{R}^n \rightarrow \mathbb{R}^n$ , which is associated with one or multiple iterations of a user-specified global optimizer. The operator  $\mathcal{K}$  takes as an input the gradient of the loss function and provides a direction  $\mathbf{p}^{(k)}$ , i.e.,  $\mathbf{p}^{(k)} := \mathcal{K}(\nabla \mathcal{L}(\boldsymbol{\theta}^{(k+1/2)}))$ . For instance, if a single step of the LBFGS optimizer is employed, then the operator  $\mathcal{K}$  is defined as

$$\mathbf{p}^{(k)} := \mathcal{K}(\nabla \mathcal{L}(\boldsymbol{\theta}^{(k+1/2)})) := -\left(\mathbf{H}^{(k+1/2)}\right)^{-1} \nabla \mathcal{L}(\boldsymbol{\theta}^{(k+1/2)}),$$

where  $\mathbf{H}^{(k+1/2)}$  denotes the Hessian approximation of  $\mathcal{L}$  at  $\boldsymbol{\theta}^{(k+1/2)}$ . Afterward, the updated global iterate  $\boldsymbol{\theta}^{(k+1)}$  is obtained as

$$\boldsymbol{\theta}^{(k+1)} = \boldsymbol{\theta}^{(k+1/2)} + \alpha^{(k)} \mathbf{p}^{(k)},$$

where  $\alpha^{(k)}$  denotes the step size, determined using the line-search globalization strategy.

**3.1. Overlapping layer-wise additive Schwarz preconditioner.** The computational cost associated with solving the preconditioned system of equations (3.3) is directly linked to the quality of the nonlinear preconditioner  $\mathcal{M}$ . In this work, we construct the preconditioner  $\mathcal{M}$  by utilizing the overlapping layer-wise network decomposition. Thus, we decompose the DNN, consisting of  $N$  layers, into  $N_{sd}$  subnetworks (subdomains), such that each layer belongs to a unique subnetwork. The parameters of the network are also decomposed into  $N_{sd}$  disjoint groups, i.e.,

$$\boldsymbol{\theta} = [\boldsymbol{\theta}_1, \dots, \boldsymbol{\theta}_s, \dots, \boldsymbol{\theta}_{N_{sd}}]^T,$$

where  $\boldsymbol{\theta}_s := [\boldsymbol{\theta}_{s,1}, \dots, \boldsymbol{\theta}_{s,N_s}]^T \in \mathbb{R}^{n_s}$ , for  $s = 1, \dots, N_{sd}$ . Each  $s^{th}$  non-overlapping subnetwork consists of  $N_s$  layers, with parameters of  $h^{th}$  layer being denoted as  $\boldsymbol{\theta}_{s,h}$ . In case of the overlapping decomposition, we concatenate parameters  $\boldsymbol{\theta}_s$  with the parameters of neighboring  $\delta (\in \mathbb{N}) < N_s$  layers from the  $(s-1)$ -th and  $(s+1)$ -th subnetworks. For  $\delta \geq 1$ , this gives rise to overlapping set of subdomain parameters

$$\tilde{\boldsymbol{\theta}}_s = [\boldsymbol{\theta}_{s-1, (N_{sd}-\delta)}, \dots, \boldsymbol{\theta}_{s-1, N_{sd}}, \boldsymbol{\theta}_{s,1}, \dots, \boldsymbol{\theta}_{s, N_{sd}}, \boldsymbol{\theta}_{s+1,1}, \dots, \boldsymbol{\theta}_{s+1, \delta}]^T \in \mathbb{R}^{\tilde{n}_s},$$

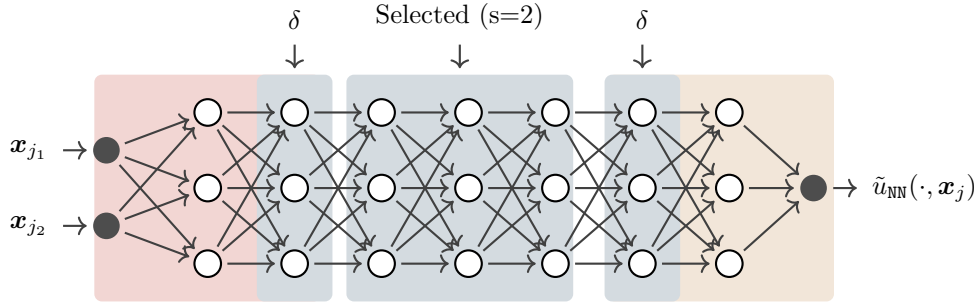


Fig. 3.1: An illustration of the network decomposed into three subdomains with overlap  $\delta = 1$ . The parameters of different color belong to different subdomains. The second subdomain (blue color,  $s = 2$ ) is selected to illustrate the overlapping subdomain parameters.

where  $\tilde{N}_s$  and  $\tilde{n}_s$  denotes the number of layers in overlapping subnetwork and the number of associated subnetwork parameters, respectively. Note that, for the first ( $s = 1$ ) and the last ( $s = N_{sd}$ -th) subnetworks, we only pick layers from the second and  $(N_{sd} - 1)$ -th subnetworks, respectively. Figure 3.1 illustrates the parameter selection for the second subnetwork of the six-layer network decomposed in a layer-wise manner into three subdomains with an overlap of size one, i.e.,  $N_{sd} = 3$  and  $\delta = 1$ .

To transfer the data between the subnetworks and the global network, we define a restriction operator  $\mathbf{R}_s: \mathbb{R}^n \rightarrow \mathbb{R}^{\tilde{n}_s}$ , which extracts the parameters of the overlapping subnetwork from the parameters of the global network, i.e.,

$$\tilde{\theta}_s = \mathbf{R}_s \theta.$$

Moreover, we also consider the prolongation operator  $\mathbf{R}_s^T: \mathbb{R}^{\tilde{n}_s} \rightarrow \mathbb{R}^n$ , defined as adjoint of  $\mathbf{R}_s$ . The role of the prolongation operator  $\mathbf{R}_s^T$  is to extend the parameters associated with  $s^{\text{th}}$  subnetwork to the global network, i.e.,  $\theta = \sum_{s=1}^{N_{sd}} \mathbf{R}_s^T \tilde{\theta}_s$ .

*Remark 3.1.* In the case of DON, we decompose the trunk and branch networks independently of each other. For instance, if  $N_{sd} = 2$ , the branch and trunk constitute two separate non-overlapping subdomains. If  $N_{sd} > 2$ , then branch and trunk networks are further decomposed into multiple, possibly overlapping, subdomains.

**3.1.1. Single-level preconditioner with layer-wise synchronization strategy.** Using the proposed overlapping network decomposition, we define the local training problems for all subdomains as

$$(3.4) \quad \tilde{\theta}_s^* := \arg \min_{\tilde{\theta}_s \in \mathbb{R}^{\tilde{n}_s}} \mathcal{L}(\tilde{\theta}_s + (\mathbf{I} - \mathbf{R}_s^T \mathbf{R}_s) \theta),$$

where  $s \in 1, \dots, N_s$ . Thus, for the  $s^{\text{th}}$  subdomain, we minimize the loss functional  $\mathcal{L}$  with respect to parameters  $\tilde{\theta}_s$ , while all other parameters are held fixed. The minimization problem (3.4) is solved only approximately, for example, by utilizing a few steps of the LBFGS or Adam optimizer. The resulting parameters  $\tilde{\theta}_s^*$  are then used to define the (single-level) overlapping additive Schwarz preconditioner  $\mathcal{M}_{SL}$  as

$$(3.5) \quad \mathcal{M}_{SL}(\theta) := \theta + \gamma \sum_{s=1}^{N_{sd}} \mathbf{R}_s^T (\tilde{\theta}_s^* - \mathbf{R}_s \theta) =: \theta + \gamma \sum_{s=1}^{N_{sd}} \mathbf{d}_s =: \theta + \gamma \mathbf{d}.$$

Here, the symbol  $\gamma \in [0, 1]$  denotes an appropriately selected damping parameter, such that

$$\mathcal{L}(\boldsymbol{\theta} + \gamma \mathbf{d}) \leq \mathcal{L}(\boldsymbol{\theta}).$$

It is crucial to note that the convergence rate of the preconditioner  $\mathcal{M}_{SL}$  is strongly affected by the value of  $\gamma$  as well as by the quality of the search direction  $\mathbf{d}$ . In the literature on the linear additively composed preconditioners, the multi-preconditioning approach [7, 24] is often employed to determine how to optimally combine locally obtained search directions  $\{\mathbf{d}_s\}_{s=1}^{N_{sd}}$  to improve the quality of the resulting search direction  $\mathbf{d}$ . Here, we extend this methodology into nonlinear settings by searching for a set of damping parameters  $\{\gamma_s^*\}_{s=1}^{N_{sd}}$ , such that

$$(3.6) \quad \mathcal{L} \left( \boldsymbol{\theta} + \sum_{s=1}^{N_{sd}} \gamma_s^* \mathbf{d}_s \right) < \mathcal{L} \left( \boldsymbol{\theta} + \sum_{s=1}^{N_{sd}} \gamma_s \mathbf{d}_s \right),$$

for all  $\gamma_s^* \neq \gamma_s$ .

The set  $\{\gamma_s^*\}_{s=1}^{N_{sd}}$  can be determined by solving the following  $N_{sd}$ -dimensional minimization problem:

$$(3.7) \quad \min_{\gamma_1, \dots, \gamma_{N_{sd}}} \mathcal{L} \left( \boldsymbol{\theta} + \sum_{s=1}^{N_{sd}} \gamma_s \mathbf{d}_s \right).$$

However, finding a solution of (3.7) is computationally demanding due to the nonlinear nature of the problem. This is in contrast to multi-preconditioning approaches used in the context of linear problems, where  $\{\gamma_s^*\}_{s=1}^{N_{sd}}$  can typically be obtained in closed form, see for instance [6, 7].

To elevate the computational burden of solving (3.7) exactly, one can employ multidimensional line-search heuristics, such as multidimensional backtracking proposed in [46]. Here, we opt for a simplified approach and leverage the fact that the majority of DNNs construct their bases by propagating the input features through the network from the first to the last layer in a sequential manner, which is frequently regarded as a time-dependent process [26, 47]. Therefore, we also follow the feature flow and determine  $\{\gamma_s^*\}_{s=1}^{N_{sd}}$  in a sequential manner, such that

$$\mathcal{L} \left( \boldsymbol{\theta} + \sum_{j=1}^{s-1} \gamma_j^* \mathbf{d}_j + \gamma_s \mathbf{d}_s \right) \leq \mathcal{L} \left( \boldsymbol{\theta} + \sum_{j=1}^{s-1} \gamma_j^* \mathbf{d}_j \right),$$

for  $s = 1, \dots, N_{sd}$ . Thus, the values  $\{\gamma_s^*\}_{s=1}^{N_{sd}}$  are determined from the first subdomain to the last one, utilizing a standard, unidimensional, line-search strategy. This guarantees that each search direction  $\mathbf{d}_s$  decreases the value of  $\mathcal{L}$  associated with a global network. At the same time, we ensure that the DNN's bases are constructed by appropriately adjusting the impact of each search direction  $\mathbf{d}_s$  on the global DNN's approximation. Here, we remark that the search directions  $\{\mathbf{d}_s\}_{s=1}^{N_{sd}}$  are obtained in parallel, while only scalar damping parameters  $\{\gamma_s^*\}_{s=1}^{N_{sd}}$  are obtained sequentially during the subdomain synchronization step.

**3.2. Two-level overlapping additive Schwarz preconditioner.** In the field of numerical methods, the convergence of single-level preconditioners is often enhanced

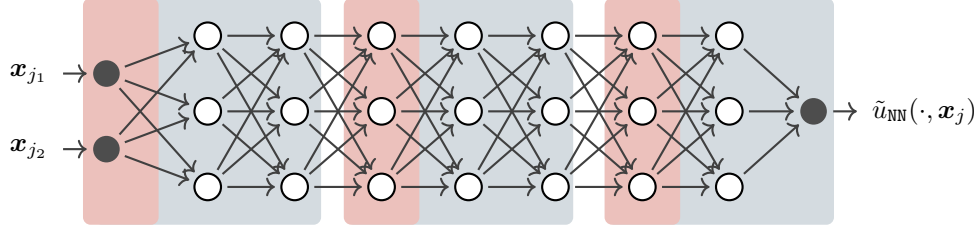


Fig. 3.2: An example of network decomposition associated with coarse level training. The first layer (red color) of each subdomain (red+blue color) is selected to construct a set of trainable coarse level parameters.

by incorporating a coarse level, which ensures a global communication between subdomains. Following this methodology, we propose to improve the convergence of a single-level layer-wise preconditioner by incorporating a coarse-level training step. Our design of the coarse-level network is inspired by the observation that the forward pass through the network can be interpreted as a time-stepping process [21, 23, 26, 43, 47]. This observation suggests that coarse-level subnetworks can be created by reducing the number of layers within a given subdomain, analogous to time-step coarsening. More precisely, we create the coarse-level subnetwork by grouping together the first layers of each subdomain. Thus, the trainable coarse-level parameters are given as

$$(3.8) \quad \boldsymbol{\theta}_0 = [\boldsymbol{\theta}_{1,1}, \dots, \boldsymbol{\theta}_{s,1}, \dots, \boldsymbol{\theta}_{N_{sd},1}]^T,$$

where  $\boldsymbol{\theta}_{s,1}$  is extracted from  $\boldsymbol{\theta}_s = [\boldsymbol{\theta}_{s,1}, \dots, \boldsymbol{\theta}_{s,\tilde{N}_s}]^T$ , for all  $s = 1, \dots, N_{sd}$ . An illustration of the coarse-level parameter selection for a six-layer network with  $N_{sd} = 3$  and  $\delta = 0$  is depicted in Figure 3.2.

The transfer of the data between the coarse-level subnetwork and the global network, is ensured by two transfer operators. In particular, we consider the restriction operator  $\mathbf{R}_0: \mathbb{R}^n \rightarrow \mathbb{R}^{n_0}$  and its adjoint, the prolongation operator  $\mathbf{R}_0^T: \mathbb{R}^{n_0} \rightarrow \mathbb{R}^n$ , given such that

$$\boldsymbol{\theta}_0 = \mathbf{R}_0 \boldsymbol{\theta}, \quad \boldsymbol{\theta} = \mathbf{R}_0^T \boldsymbol{\theta}_0.$$

Note that the number of trainable coarse-level parameters  $n_0$  scales proportionally to the number of subdomains  $N_{sd}$ .

Using the coarse-level subnetwork, we can now define the coarse-level training problem as

$$\boldsymbol{\theta}_0^* := \arg \min_{\boldsymbol{\theta}_0 \in \mathbb{R}^{n_0}} \mathcal{L}(\boldsymbol{\theta}_0 + (\mathbf{I} - \mathbf{R}_0^T \mathbf{R}_0) \boldsymbol{\theta}).$$

Hence, the loss functional  $\mathcal{L}$  is minimized with respect to the parameters associated with the coarse-level subnetwork while all other parameters are held fixed. The outcome of the coarse-level minimization process, the parameters  $\boldsymbol{\theta}_0^* \in \mathbb{R}^{n_0}$ , is then used to update the parameters of the global network as

$$(3.9) \quad \hat{\boldsymbol{\theta}} = \boldsymbol{\theta} + \mathbf{R}_0^T (\boldsymbol{\theta}_0^* - \mathbf{R}_0 \boldsymbol{\theta}).$$

Note that since all coarse-level parameters  $\boldsymbol{\theta}_0$  are optimized simultaneously, the coarse-level training process is serial. Moreover, the condition  $\mathcal{L}(\hat{\boldsymbol{\theta}}) \leq \mathcal{L}(\boldsymbol{\theta})$  is automatically fulfilled.



Table 4.1: The summary of network architectures for PINN’s benchmark problems.

Example	Layers	Act.
Burg	FNN[2, 20, 20, 20, 20, 20, 20, 1]	Tanh
DA	FNN[2, 50, 50, 50, 50, 50, 50, 50, 1]	Tanh
AC	FNN[2, 32, 32, 32, 32, 32, 32, 32, 32, 1]	Tanh

- **Burgers’ equation (Burg):** Burgers’ equation is given in the following form:

$$\begin{aligned} \frac{\partial u}{\partial t} + uu' - \nu u'' &= 0, & \forall (t, x) \in (0, 1] \times (-1, 1), \\ u &= -\sin(\pi x), & \forall (t, x) \in \{0\} \times [-1, 1], \\ u &= 0, & \forall (t, x) \in (0, 1] \times \{1\}, \\ u &= 0, & \forall (t, x) \in (0, 1] \times \{-1\}, \end{aligned}$$

where  $u = u(t, x)$  denotes the flow velocity and  $\nu$  stands for the kinematic viscosity. Here, we choose  $\nu = 0.01/\pi$ .

- **Diffusion-advection (DA):** The diffusion-advection equation is given as

$$\begin{aligned} -\mu \Delta u + \mathbf{b} \cdot \nabla u &= f, & \forall (x_1, x_2) \in (0, 1) \times (0, 1), \\ u &= 0, & \text{on } \partial\Omega, \end{aligned}$$

where  $\mathbf{b} = (1, 1)^\top$ . The right-hand side is considered to be constant, i.e.,  $f = 1$ . Moreover, the symbol  $\mu$  denotes viscosity, which we choose to set as  $\mu = 10^{-2}$ .

- **Allen-Cahn (AC):** We consider the Allen-Cahn equation of the following form:

$$\begin{aligned} \frac{\partial u}{\partial t} - Du'' - 5(u - u^3) &= 0, & \forall (t, x) \in (0, 1] \times (-1, 1), \\ u &= x^2 \cos(\pi x), & \forall (t, x) \in \{0\} \times [-1, 1], \\ u &= -1, & \forall (t, x) \in (0, 1] \times \{-1\}, \\ u &= -1, & \forall (t, x) \in (0, 1] \times \{1\}, \end{aligned}$$

where the diffusion coefficient  $D$  is chosen as  $D = 0.001$ .

The amount and location of collocation points significantly influence the discretization error of PINNs. Here, we perform sampling by employing the quasi-Monte Carlo method [57], with Hammersley low-discrepancy sequences [56]. As a consequence, the convergence rate of Quasi-Monte Carlo is close to  $O(N^{-1})$ , whereas the convergence rate of the standard Monte Carlo method, with pseudorandom sequences, is  $O(N^{-1/2})$  [3]. The number of collocation points is 10,000 for all three examples.

**4.2. Benchmark problems for training of DONs.** For the training of DONs, we consider the three benchmark problems, with datasets created using the finite element method within the Firedrake library [27].

- **Anisotropic Poisson equation (Aniso):** Let  $\Omega := (-1, 1)^2$  be the computational domain, with boundary  $\partial\Omega$ , the anisotropic Poisson equation is given as

$$(4.1) \quad \begin{aligned} -\nabla \cdot (K(x, \boldsymbol{\eta}) \nabla u(x)) &= f(x), & \forall x \in \Omega, \\ u &= 0, & \forall x \in \partial\Omega, \end{aligned}$$

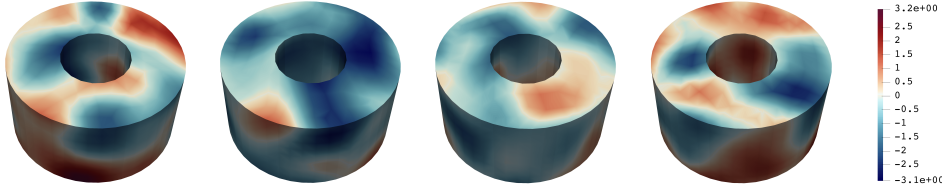


Fig. 4.1: Example of sampled right-hand sides for creating the Helm dataset.

where  $u$  denotes the solution and  $f(x) := 1$  is the forcing term. The diffusion coefficient  $K(x, \boldsymbol{\eta})$  is considered to be anisotropic tensor of the following form:

$$K(x, \boldsymbol{\eta}) = \begin{pmatrix} \cos(\alpha) & -\sin(\alpha) \\ \sin(\alpha) & \cos(\alpha) \end{pmatrix} \begin{pmatrix} 1 & 0 \\ 0 & \beta \end{pmatrix} \begin{pmatrix} \cos(\alpha) & \sin(\alpha) \\ -\sin(\alpha) & \cos(\alpha) \end{pmatrix},$$

where  $\boldsymbol{\eta} := [\alpha, \beta]$ . The parameter  $\beta \in [10^{-6}, 1]$  specifies the anisotropic strength, and it is sampled from the following distribution:  $\log_{10}(1/\beta) \sim \mathcal{U}[0, 6]$ . The parameter  $\alpha \in (0, \pi)$ , sampled as  $\alpha \sim \mathcal{U}[0, \pi]$ , is used to specify the angle of anisotropic direction. The components of the forcing term are selected randomly from the Gaussian distribution  $\mathcal{N}(0, 1)$ . To construct the dataset, for each  $\boldsymbol{\alpha}$ , we discretize (4.1) using uniform mesh with  $34 \times 34$  elements. The number of training samples and test samples are 4,250 and 750, respectively. We have uploaded this new dataset to the public ZENODO repository [38].

- **Helmholtz equation (Helm):** Let  $\Omega$  be the computational domain, defined as an annular cylinder depicted on Figure 4.1. The parametrized Helmholtz equation is given as

$$(4.2) \quad \begin{aligned} -\Delta u(x) - k_{\text{H}}^2 u(x) &= f(x, \boldsymbol{\eta}), & \forall x \in \Omega, \\ u &= 0, & \forall x \text{ on } \partial\Omega_T, \end{aligned}$$

where  $u$  is the solution and  $\Omega_T$  denotes the top boundary of the cylinder. Moreover, the symbol  $k_{\text{H}}$  denotes a constant wave number, which we set to  $k_{\text{H}} = 3$ . We sample the forcing term from Gaussian random fields (GRFs) with mean  $\mathbb{E}[f(x, \boldsymbol{\eta})] = 0$ , and the covariance is given as

$$\text{Cov}(f(x, \boldsymbol{\eta}), f(y, \boldsymbol{\eta})) = \sigma^2 \exp\left(-\frac{\|x - y\|^2}{2\ell^2}\right),$$

with  $\sigma = 3.0$  and  $\ell = 0.1$ . To construct the dataset, we discretize (4.2) using an unstructured mesh with 1,503 nodes. The sampled right-hand sides are then interpolated to the bounding box  $[-1, 1] \times [-1, 1] \times [0, 1]$ , consisting of  $32 \times 32 \times 32$  elements, to create a representation that 3D convolutional layers of the branch network can efficiently process. The number of training samples and test samples are 4,250 and 750, respectively. We have made this new dataset publicly accessible on the ZENODO repository [39].

- **Advection equation (Adv):** Following [53], we consider a wave advection equation with periodic boundary conditions, defined at the domain  $\Omega := [0, 1]$  in space and  $[0, 1]$  in time. The problem is parameterized with respect to different initial

Table 4.2: The summary of network architectures for DON’s benchmark problems. The symbol  $[\cdot]$  indicates the number of channels for CNN and the width for FNN, respectively. The symbols B and T denote the branch network and trunk network, respectively.

Example		Layers	Act.
Aniso	B	FNN[2, 256, 256, 256, 256, 128]	ReLU
	T	FNN[2, 256, 256, 256, 128]	Tanh
Helm	B	CNN[1, 40, 60, 100, 180] + FNN[180, 80, 80, 80, 128]	ReLU
	T	FNN[3, 80, 80, 80, 128]	Tanh
Adv	B	FNN[40, 64, 64, 64, 64, 64, 64, 32]	ReLU
	T	POD-basis	-

conditions, and it is given as

$$\begin{aligned} \frac{\partial u}{\partial t} + \frac{\partial u}{\partial x} &= 0, & \forall (x, t) \in \Omega \times [0, 1], \\ u &= u_0(x, \boldsymbol{\eta}), & \forall (x, t) \in \Omega \times \{0\}. \end{aligned}$$

The DON is trained to learn a map from the initial condition to the solution of PDE. To this aim,  $u_0$  is parametrized as  $u_0(x, \boldsymbol{\eta}) := h_1 1_{\{c_1 - \frac{w}{2}, c_1 + \frac{w}{2}\}} + \sqrt{\max(h_2^2 - a^2(x - c_2)^2, 0)}$ , where the parameters  $\boldsymbol{\eta} := [a, h_1, h_2, c_1, c_2, w]$  are sampled randomly from the range  $[0.1, 0.2]$ ,  $[0.5, 2.0]$ ,  $[0.5, 2.0]$ ,  $[0.2, 0.3]$ ,  $[0.7, 0.8]$ , for  $a, h_1, h_2, c_1, c_2$  and  $w$ , respectively. The dataset for training the DON is constructed using a finite difference method with uniform mesh composed of  $40 \times 40$  nodes in space-time. The number of training and test samples is 1,000. Note that for this benchmark problem, we utilize the POD-DeepONet architecture [53], which replaces the trunk network with the POD bases. This allows us to effectively demonstrate the capabilities of the proposed layer-wise decomposition for different types of DON architectures.

**4.3. Implementation details.** All benchmark problems and considered optimizers are implemented on top of the library PyTorch [59]. The code used for generating the numerical results is part of the open-source library DistTrainN [42]. The description of DNN architectures is summarized in Table 4.1 and Table 4.2 for PINNs and DONs, respectively. All networks are initialized using Xavier initialization strategy [22]. For PINNs, the boundary conditions are imposed by employing the length factor function  $\ell$  given as  $\ell(x_1, x_2) = x_1(1 - x_1)x_2(1 - x_2)$  and  $\ell(t, x) = t(x + 1)(x - 1)$  for DA problem and Burg/AC problems, respectively. Moreover, we employ an adaptive activation function [33] and a skip-connection [28].

As a baseline, we employ the LBFGS optimizer and single-level layer-wise preconditioned LBFGS (SL-BFGS). The proposed two-level preconditioner is also tested by preconditioning the LBFGS method, giving rise to the TL-BFGS optimizer. All LBFGS variants utilize the limited-memory implementation with the memory size  $m = 3$ . Moreover, we utilize momentum with parameter 0.9 and the cubic backtracking line-search with strong Wolfe conditions [14, Algorithm A6.3.1, pages 325-327] to obtain all step-sizes. For the SL/TL-LBFGS optimizers, the global and local optimization problems outlined in Algorithm 3.1, are also solved using the LBFGS, which is restarted at every epoch.

Table 4.3: Estimates for the number of the gradient evaluations ( $g_e$ ), update cost (UC), and memory requirements (MC) per iteration for the LBFGS and the TL-LBFGS optimizers. The bold symbol denotes the iteration cost associated with incorporating the coarse-level training, i.e., additional cost compared to SL-LBFGS.

Method	$g_e$	UC	MC
LBFGS	1	$n + 4mn$	$n + 2mn$
TL-LBFGS	$2 + k_s(g_{e_s}) + \mathbf{k_0(g_{e_0})}$	$2n + 4mn + (\tilde{n}_s/n)k_s\text{UC}_s + \mathbf{(n_0/n)k_0\text{UC}_0}$	$2n + 2mn + (\tilde{n}_s/n)\text{MC}_s + \mathbf{(n_0/n)\text{MC}_0}$

Compared to the standard LBFGS algorithm, a single iteration/epoch of the TL-LBFGS method is computationally more expensive. To analyze the iteration cost, Table 4.3 summarizes the gradient evaluations cost ( $g_e$ ), the update cost (UC) and memory cost (MC) of the LBFGS and TL-LBFGS optimizers. As we can see, the LBFGS optimizer requires one gradient evaluation per iteration, i.e.,  $g_e = 1$ . However, UC depends on the size of stored secant pairs ( $m$ ) used for Hessian approximation. It can be approximately estimated as  $4mn$  flops when the compact matrix representation is employed; see [8, Sections 3 and 4] for details. By incorporating the cost associated with evaluating the momentum, the UC equals to  $n + 4mn$  flops. In the perspective of MC, the LBFGS optimizer requires storing two matrices of size  $m \times n$  as well as a momentum of length  $n$ , which takes up memory of size  $n + 2mn$ .

The computational cost of the TL-LBFGS optimizer is associated with global, local and coarse-level training phases. The global computational cost is exactly same as for the standard LBFGS optimizer. The gradient evaluation cost for local and coarse-level parts are  $k_s g_{e_s}$  and  $k_0 g_{e_0}$ , where ( $g_{e_s}$ ) and ( $g_{e_0}$ ) denote the cost of gradient evaluation of local and coarse-level optimizers, respectively. Since the number of coarse trainable parameters is the number of subdomain  $N_{sd}$ , the cost of coarse-level evaluation  $g_{e_0}$  is generally less than that of local evaluation  $g_{e_s}$ . In terms of UC, let  $\text{UC}_s$  and  $\text{UC}_0$  be the update cost required by the local and coarse optimizers. Since the UC for  $s^{\text{th}}$  subnetwork is scaled proportionally to the number of local trainable parameters  $n_s$  and the number of local iterations  $k_s$ , the local update cost is  $(\tilde{n}_s/n)k_s\text{UC}_s$ . Similarly, the coarse-level update cost is  $(n_0/n)k_0\text{UC}_0$ . Note that MC of TL-LBFGS can be derived similarly to the derivation of UC, i.e., the local memory cost and the coarse-level memory cost are  $(\tilde{n}_s/n)\text{MC}_s$  and  $(n_0/n)\text{MC}_0$ , respectively.

**5. Numerical results.** In this section, we investigate the performance of the proposed TL-LBFGS preconditioner. To this aim, we monitor the value of the loss function  $\mathcal{L}$  and the relative  $L^2$  error, given as

$$\mathcal{E}_{\text{rel}}(u_{\theta}, u^*) = \frac{\|u_{\theta} - u^*\|_{L^2(\Omega)}}{\|u_{\theta}\|_{L^2(\Omega)}},$$

where  $u_{\theta}$  is the neural network solution and  $u^*$  denotes the exact or the high-fidelity finite element solution.

**5.1. Impact of the overlap on the convergence of SL-LBFGS.** First, we investigate the impact of overlap on the convergence of the SL-LBFGS optimizer. During this experiment, we fix the number of local iterations at  $k_s = 50$  and consider a varying number of subnetworks  $N_{sd} \in \{2, 4, 8\}$  and the size of the overlapping

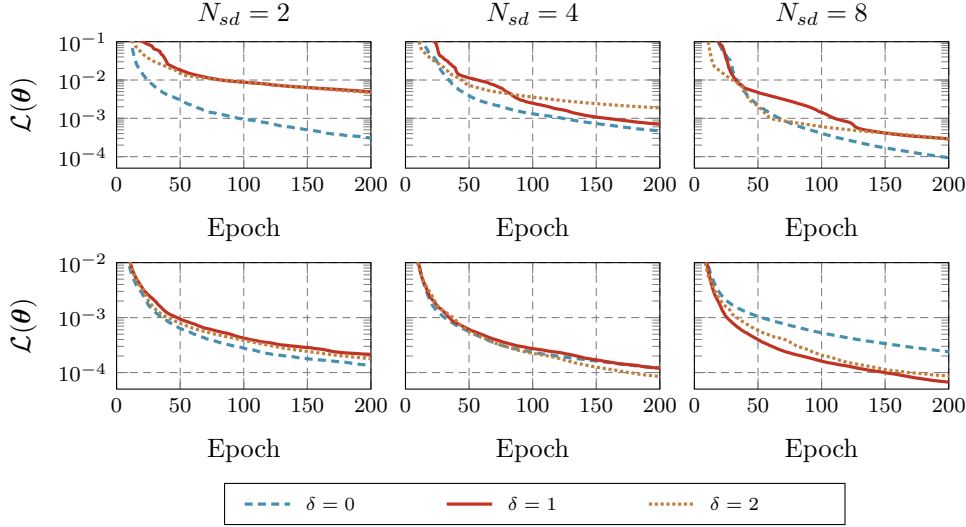


Fig. 5.1: The convergence of the SL-LBFGS method for Burg (Top) and Adv (Bottom) with respect to various  $N_{sd}$  and  $\delta$ . The parameters corresponding to the overlapping regions are averaged, i.e., the layer-wise subdomain synchronization strategy is not used. The results are obtained over 5 independent runs.

regions  $\delta \in \{0, 1, 2\}$ . **Figure 5.1** illustrates the obtained results for Burg (PINN) and the Adv (DON) equations. Note, the layer-wise synchronization strategy proposed in Section 3.1.1 is not utilized. Instead, we average the parameters of the layers corresponding to the overlap, an approach traditionally used in numerical analysis. As we can see from the obtained results, in this particular case, increasing the size of the overlap  $\delta$  does not improve convergence, and in some cases, it even causes its deterioration.

For comparison, **Figure 5.2** demonstrates the obtained results by incorporating the novel layer-wise synchronization strategy. In contrast to the results reported in **Figure 5.1**, we can observe that using the layer-wise synchronization strategy allows for an enhanced convergence as the size of the overlapping region  $\delta$  increases. Here, we, however, point out that as  $\delta$  increases, the computational cost of solving the local minimization problems also increases. Consequently, selecting  $\delta = 1$  provides the best trade-off between enhanced convergence and the low computational cost.

**5.2. Impact of coarse-level training (SL-LBFGS vs. TL-LBFGS).** As a next step, we investigate the impact of coarse-level training on the convergence of the proposed preconditioner. In this experiment, we fix the size of the overlap to  $\delta = 1$  and the number of local iterations to  $k_s = 50$ . At the same time, we vary the number of coarse-level iterations  $k_0$  and the number of subdomains  $N_{sd}$ , such that  $k_0 \in \{0, 25, 50\}$  and  $N_{sd} \in \{2, 4, 8\}$ . **Figure 5.3** illustrates the obtained results. As we can see, the loss function decays more rapidly as the number of coarse iterations  $k_0$  increases, suggesting that incorporating coarse-level training significantly improves the convergence rate of the proposed TL-LBFGS method. However, because the coarse-level training process is sequential and cannot be parallelized, an increased number of coarse-level iterations increases the computational cost. As a consequence,

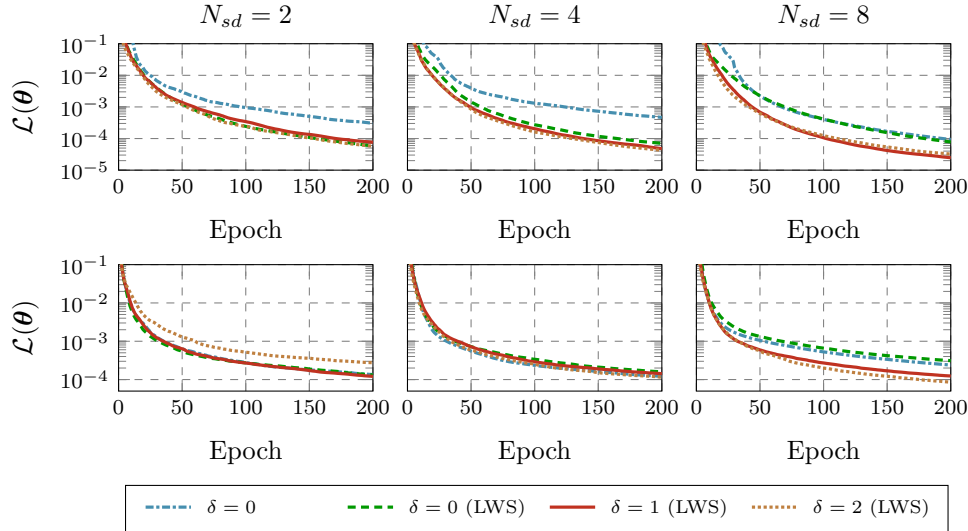


Fig. 5.2: The convergence of SL-LBFGS method for Burg (Top) and Adv (Bottom) with respect to various  $N_{sd}$  and  $\delta$ . The layer-wise synchronization (LWS) strategy introduced in subsection 3.1.1 is utilized. The results are obtained over 5 independent runs.

to achieve the tradeoff between the computational cost and the improvement in the convergence speed, we keep  $k_0$  fairly low for all subsequent numerical experiments, i.e., between 25 and 50.

**5.3. Convergence, accuracy and computational cost of the LBFGS, and SL/TL-LBFGS optimizers.** In this section, we compare the performance of the proposed TL-LBFGS optimizer with the standard LBFGS optimizer. The comparison is performed with respect to relative error  $\mathcal{E}_{\text{rel}}$ , the number of epochs,  $g_e$  and UC, as discussed in Section 4.3. Figure 5.4 and Figure 5.5 demonstrate the obtained results for PINN’s and DON’s benchmark problems. As we can see, TL-LBFGS always provides the models with lower  $\mathcal{E}_{\text{rel}}$  than the LBFGS optimizer. For example, for the DA example with  $N_{sd} = 5$ , the relative error  $\mathcal{E}_{\text{rel}}$  almost immediately decreases to  $10^{-2}$ , while LBFGS optimizer fails to train the model to that accuracy. Moreover, we can also observe that for all benchmark problems, the performance of TL-LBFGS improves as the number of subdomains  $N_{sd}$  increases.

As a next step, we compare the performance of TL-LBFGS with respect to its single-level counterpart, SL-LBFGS. We configure SL-LBFGS as proposed in [40], i.e., without overlap, without layer-wise synchronization strategy and without the coarse-level training. As we can see from Table 5.1, except in the case of Aniso problem, the TL-LBFGS method consistently outperforms the SL-LBFGS method by providing more accurate DNN models. While the observed improvements compared to the LBFGS method are around one order of magnitude, they are not as big as those compared to the SL-LBFGS method. However, in some cases, such as the Burg benchmark problem, where SL-LBFGS did not perform very well <sup>2</sup>, TL-LBFGS yields

<sup>2</sup>For Burg problem, the SL-LBFGS method starts stagnating after 6,000 epochs at  $\mathcal{E}_{\text{rel}} = 2 \times 10^{-4}$ .

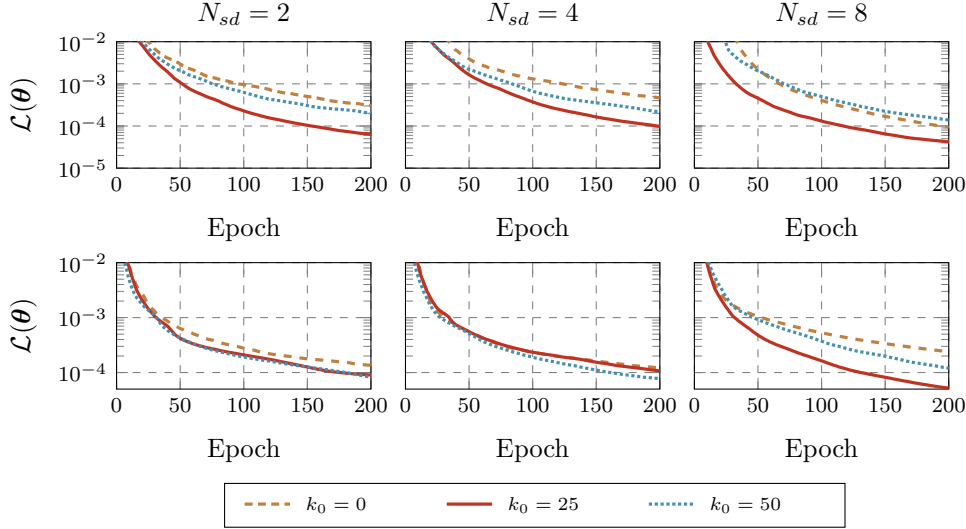


Fig. 5.3: The convergence of SL-LBFGS ( $k_0 = 0$ ) and TL-LBFGS ( $k_0 \in \{25, 50\}$ ) for Burg (Top) and Adv (Bottom) for various  $N_{sd}$ . Note that  $\delta = 0$  and the classical synchronization method described in (3.5) is used. The results are obtained over 5 independent runs.

Table 5.1: Left: The best relative error  $\mathcal{E}_{\text{rel}}$  which is achieved by LBFGS, and SL/TL-LBFGS optimizers for PINN’s (AC, DA, Burg) and DON’s (Aniso, Adv, Helm) benchmark problem. The results are obtained over 5 independent runs. Right: An overview of hyperparameters chosen for testing the SL/TL-LBFGS methods. The symbols  $N_{sd}$ ,  $k_s$ , and  $k_0$  stand for the number of subnetworks, the number of iterations for the local problems, and the number of iterations for the coarse problems, respectively.

Ex.	$\mathcal{E}_{\text{rel}}$			Hyperparameters		
	LBFGS	SL-LBFGS	TL-LBFGS	$N_{sd}$	$k_s$	$k_0$
AC	$3.6 \times 10^{-3}$	$2.4 \times 10^{-4}$	<b><math>1.6 \times 10^{-4}</math></b>	2, 6	50	50
DA	$5.5 \times 10^{-1}$	$2.2 \times 10^{-2}$	<b><math>1.8 \times 10^{-2}</math></b>	2, 5	50	25
Burg	$1.5 \times 10^{-4}$	$1.2 \times 10^{-4}$	<b><math>2.9 \times 10^{-5}</math></b>	2, 4	50	25
Aniso	$1.7 \times 10^{-2}$	<b><math>2.5 \times 10^{-3}</math></b>	$2.9 \times 10^{-3}$	2, 5	50	50
Adv	$3.0 \times 10^{-2}$	$1.9 \times 10^{-2}$	<b><math>1.1 \times 10^{-2}</math></b>	2, 4	50	50
Helm	$7.3 \times 10^{-2}$	$2.2 \times 10^{-2}$	<b><math>1.7 \times 10^{-2}</math></b>	2, 6	25	25

about four times more accurate results.

In the end, we compare  $g_e$  and UC required to achieve the same accuracy as the LBFGS optimizer. Tables 5.2 and 5.3 report the obtained results in terms of speedup factor  $\mathcal{S}$ , defined as  $\mathcal{S}_B^A = C_A/C_B$ , where  $C_A$  and  $C_B$  denote the  $g_e$  or UC required by the optimizer A and by the optimizer B, respectively. As we can see, for PINN’s problems, which are significantly more ill-conditioned than DON’s problems, utilizing the TL-LBFGS optimizer reduces  $g_e$  and UC by factors of 1.5–1,099 and 3.5–12,121

Therefore, its overall performance to achieve the same  $\mathcal{E}_{\text{rel}}$  as the LBFGS method is poor, despite being very efficient in the initial training phase.

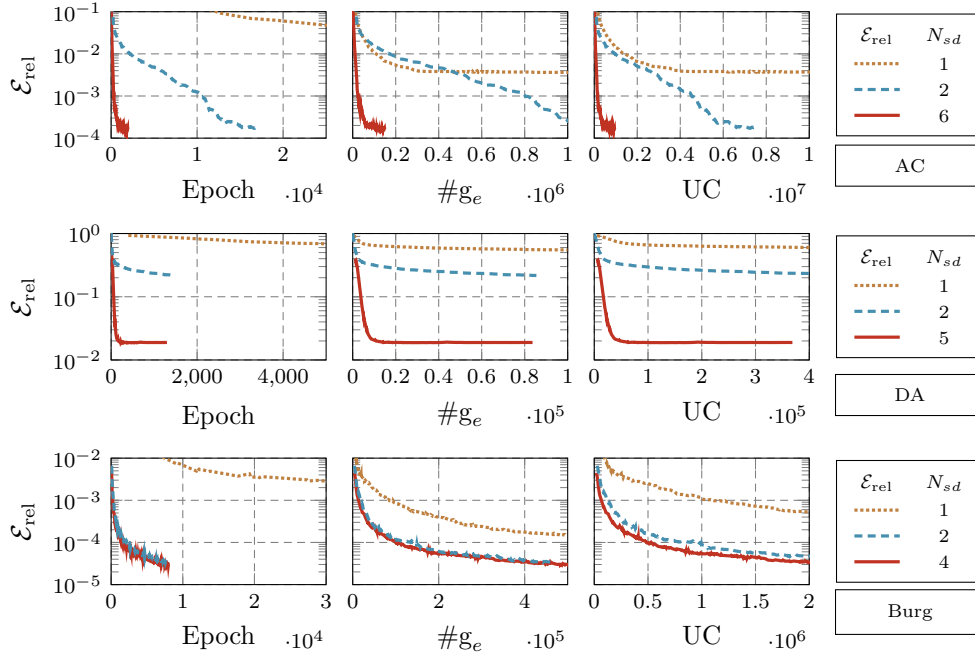


Fig. 5.4: The convergence of LBFGS ( $N_{sd} = 1$ ) and TL-LBFGS ( $N_{sd} = \{2, 5, 6\}$ ) optimizers for training PINN's benchmark problems with respect to epoch (left),  $g_e$  (middle), and UC (right). Note that a total of 32, 10, and 8 layers are used for the AC, DA, Burg problems, respectively. For TL-LBFGS, the size of the overlapping region is  $\delta = 1$ . The results are obtained over 5 independent runs.

compared to the LBFGS method, respectively. Moreover, compared to SL-LBFGS, we achieve a speedup of 2.9 – 7.3 and 1.6 – 5.1 for  $g_e$  and UC, respectively. This effectively highlights the benefits of incorporating the proposed coarse-level training step, overlap, and layer-wise synchronization into the training process.

For DON's benchmark problems, we observe lower speedup factors than for the PINNs. In particular, compared to LBFGS, we obtain speedup factors of 12.8 – 18.3 for  $g_e$  and 33.2 – 45.5 for UC, respectively. Compared to SL-LBFGS, we notice speedup factors of 0.64 – 1.7 for  $g_e$  and 0.3 – 1.3 for UC, respectively. The most unsatisfactory result is obtained for the Aniso example, where we even observe an increase in the computational cost. We attribute this behavior to the fact that this problem is the least ill-conditioned of all our benchmark problems, see [Appendix A](#). As a consequence, constructing a two-level preconditioner significantly increases the computational cost, while the convergence speed improves only slightly.

**6. Conclusion.** In this paper, we proposed a novel two-level overlapping additive Schwarz preconditioner for enhanced training of scientific machine learning applications. Motivated by traditional DD methods, the network parameters were decomposed into overlapping groups. The parameters of each group were then trained simultaneously, i.e., in parallel. To achieve fast convergence, we introduced a subdomain-wise synchronization strategy and incorporated a coarse-level training step. The performance of the devised two-level preconditioner was investigated using six benchmark

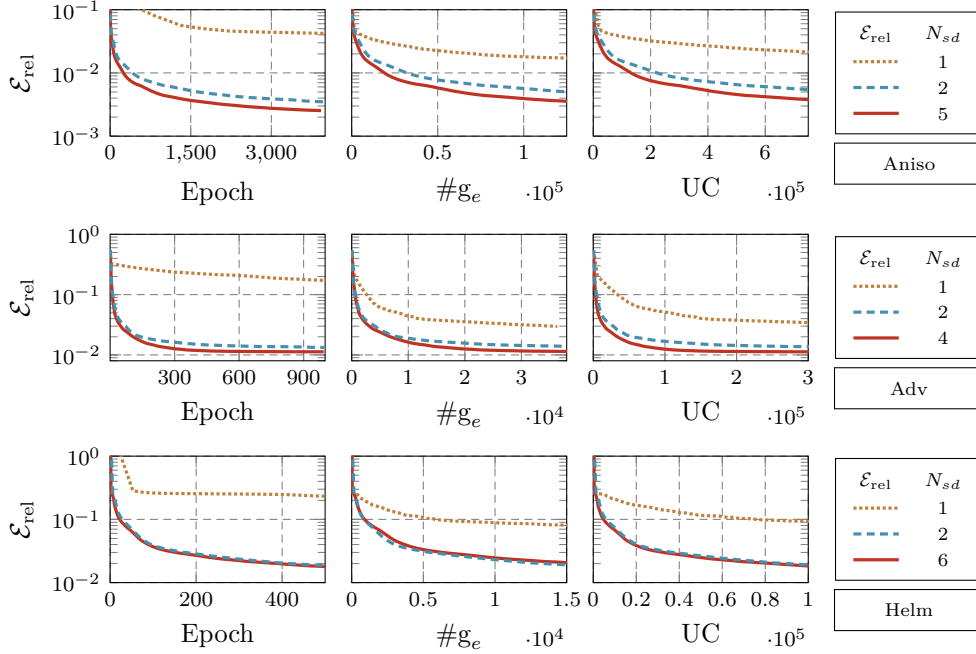


Fig. 5.5: The convergence of LBFGS ( $N_{sd} = 1$ ) and TL-LBFGS ( $N_{sd} = \{2, 5, 6\}$ ) optimizers for training DON’s benchmark problems with respect to epoch (left),  $g_e$  (middle), and UC (right). Standard DeepONet is used for Aniso and Helm, while POD-DeepONet is used for Adv. In addition, a total of 10, 12, and 8 layers are used for the Aniso, Helm, and Adv problems, respectively. For TL-LBFGS, the size of the overlapping region is  $\delta = 1$ . The results are obtained over 5 independent runs.

problems, encompassing PINNs and DONs. The obtained results demonstrated that the proposed preconditioned optimizer yields significantly more accurate models while also reducing the training cost compared to the state-of-the-art LBFGS method and the existent single-level layer-wise preconditioner.

In the future, we plan to combine the proposed two-level layer-wise preconditioning framework with approaches that consider the decomposition of the computational domain/data space, such as those proposed in [17, 32]. Moreover, it would be interesting to extend the proposed training algorithm into stochastic settings, which would enable its applicability beyond scientific machine learning applications. Furthermore, developing strategies for enhanced parallel implementation, such as load balancing and optimization of the subnetwork’s loss/gradient evaluations, could further improve the performance.

#### Appendix A. Condition number of (layer-wise) neural tangent kernel.

Table A.1 reports the condition number of neural tangent kernel (NTK) [12, 31], denoted by  $\text{cond}(\mathbb{A})$  for all benchmark problems considered in Section 4. As we can see, the problems associated with training PINNs are more ill-conditioned than those associated with training DONs. Moreover, we also see that for PINN problems, the layer-wise condition number, denoted by  $\text{cond}(\mathbb{A}_l)$ , varies over a wider range. This suggests that the local training associated with solving (3.4) requires different

Table 5.2: The number of gradient evaluation ( $g_e$ ) required by LBFGS and SL/TL-LBFGS optimizers for achieving the same relative error  $\mathcal{E}_{\text{rel}}$  as obtained by the LBFGS optimizer. The results are obtained over 5 independent runs. The speedup factor  $\mathcal{S}$  is defined as  $\mathcal{S}_B^A = g_e^A/g_e^B$ , where  $g_e^A$  and  $g_e^B$  denote the  $g_e$  required by the optimizer A and by the optimizer B.

Ex.	$\mathcal{E}_{\text{rel}}$ (LBFGS)	$g_e$					
		LBFGS	SL	$\mathcal{S}_{\text{LBFGS}}^{\text{SL}}$	TL	$\mathcal{S}_{\text{LBFGS}}^{\text{TL}}$	$\mathcal{S}_{\text{SL}}^{\text{TL}}$
AC	$3.6 \times 10^{-3}$	1,090,134	49,296	22.11	<b>16,786</b>	64.9	2.9
DA	$5.5 \times 10^{-1}$	497,000	1,560	318.5	<b>452</b>	1,099.5	3.5
Burg	$1.5 \times 10^{-4}$	99,900	553,332	0.2	<b>75,014</b>	1.5	7.3
Aniso	$1.7 \times 10^{-2}$	130,623	<b>4,784</b>	27.3	7,392	17.7	0.64
Adv	$3.0 \times 10^{-2}$	36,338	5,044	7.2	<b>2,838</b>	12.8	1.7
Helm	$7.3 \times 10^{-2}$	29,965	2,673	11.2	<b>1,638</b>	18.3	1.6

Table 5.3: The update cost (UC) required by LBFGS and SL/TL-LBFGS optimizers for achieving the same relative error  $\mathcal{E}_{\text{rel}}$  as obtained by the LBFGS optimizer. The results are obtained over 5 independent runs. The speedup factor  $\mathcal{S}$  is defined as  $\mathcal{S}_B^A = \text{UC}^A/\text{UC}^B$ , where  $\text{UC}^A$  and  $\text{UC}^B$  denote the UC required by the optimizer A and by the optimizer B.

Ex.	$\mathcal{E}_{\text{rel}}$ (LBFGS)	UC					
		LBFGS	SL	$\mathcal{S}_{\text{LBFGS}}^{\text{SL}}$	TL	$\mathcal{S}_{\text{LBFGS}}^{\text{TL}}$	$\mathcal{S}_{\text{SL}}^{\text{TL}}$
AC	$3.6 \times 10^{-3}$	14,171,742	167,322	84.7	<b>106,580</b>	132.9	1.6
DA	$5.5 \times 10^{-1}$	6,461,000	4,154	1555.4	<b>533</b>	12,121.9	2.9
Burg	$1.5 \times 10^{-4}$	1,298,700	1,878,137	0.69	<b>365,496</b>	3.5	5.1
Aniso	$1.7 \times 10^{-2}$	1,698,099	<b>13,248</b>	128.2	51,168	33.2	0.3
Adv	$3.0 \times 10^{-2}$	472,394	16,072	29.4	<b>14,130</b>	33.4	1.1
Helm	$7.3 \times 10^{-2}$	389,545	11,400	34.2	<b>8,560</b>	45.5	1.3

adjustments of step-size. Thus, by decoupling the layers, we are able to use larger step-sizes for layers that are better conditioned, which in turn enhances the overall convergence.

## REFERENCES

- [1] S. J. ANAGNOSTOPOULOS, J. D. TOSCANO, N. STERGIOPULOS, AND G. E. KARNIADAKIS, *Residual-based attention in physics-informed neural networks*, Computer Methods in Applied Mechanics and Engineering, 421 (2024), p. 116805.
- [2] A. ANANDKUMAR, K. AZIZZADENESHELI, K. BHATTACHARYA, N. KOVACHKI, Z. LI, B. LIU, AND A. STUART, *Neural operator: Graph kernel network for partial differential equations*, in ICLR 2020 Workshop on Integration of Deep Neural Models and Differential Equations, 2020.
- [3] S. ASMUSSEN AND P. W. GLYNN, *Stochastic simulation: algorithms and analysis*, vol. 57, Springer New York, NY, 2007.
- [4] A. R. BARRON, *Universal approximation bounds for superpositions of a sigmoidal function*, IEEE Transactions on Information Theory, 39 (1993), pp. 930–945.
- [5] T. BEN-NUN AND T. HOEFLER, *Demystifying parallel and distributed deep learning: An in-depth concurrency analysis*, ACM Computing Surveys (CSUR), 52 (2019), pp. 1–43.
- [6] C. BREZINSKI, *Multiparameter descent methods*, Linear Algebra and its Applications, 296 (1999), pp. 113–141.

Table A.1: Average condition number of the NTK for all benchmark problems.

Ex.	$\approx \log(\text{cond}(\mathbb{A}))$	Layer-wise $\approx \log(\text{cond}(\mathbb{A}_l))$	
		min	max
AC	26	21	27
DA	23	20	26
Burg	33	29	36
Aniso	23	21	23
Adv	22	15	22
Helm	21	18	21

- [7] R. BRIDSON AND C. GREIF, *A multipreconditioned conjugate gradient algorithm*, SIAM Journal on Matrix Analysis and Applications, 27 (2006), pp. 1056–1068.
- [8] R. H. BYRD, J. NOCEDAL, AND R. B. SCHNABEL, *Representations of quasi-Newton matrices and their use in limited memory methods*, Mathematical Programming, 63 (1994), pp. 129–156.
- [9] X.-C. CAI, D. E. KEYES, AND L. MARCINKOWSKI, *Non-linear additive schwarz preconditioners and application in computational fluid dynamics*, International Journal for Numerical Methods in Fluids, 40 (2002), pp. 1463–1470.
- [10] F. CHAOUQUI, M. J. GANDER, P. M. KUMBHAR, AND T. VANZAN, *Linear and nonlinear substructured restricted additive Schwarz iterations and preconditioning*, Numerical Algorithms, 91 (2022), pp. 81–107.
- [11] T. CHEN, H. CHEN, AND R.-W. LIU, *A constructive proof of Cybenko’s approximation theorem*, in Computing Science and Statistics, Springer New York, NY, 1992, pp. 163–168.
- [12] T. DE RYCK, F. BONNET, S. MISHRA, AND E. DE BÉ ZENAC, *An operator preconditioning perspective on training in physics-informed machine learning*, in The Twelfth International Conference on Learning Representations, 2024.
- [13] J. DEAN, G. CORRADO, R. MONGA, K. CHEN, M. DEVIN, M. MAO, M. A. RANZATO, A. SENIOR, P. TUCKER, K. YANG, Q. LE, AND A. NG, *Large scale distributed deep networks*, in Advances in Neural Information Processing Systems, vol. 25, 2012, pp. 1223–1231.
- [14] J. E. DENNIS AND R. B. SCHNABEL, *Numerical Methods for Unconstrained Optimization and Nonlinear Equations*, SIAM Philadelphia, 1996.
- [15] V. DOLEAN, M. J. GANDER, W. KHERIJI, F. KWOK, AND R. MASSON, *Nonlinear preconditioning: How to use a nonlinear Schwarz method to precondition Newton’s method*, SIAM Journal on Scientific Computing, 38 (2016), pp. A3357–A3380.
- [16] V. DOLEAN, A. HEINLEIN, S. MISHRA, AND B. MOSELEY, *Multilevel domain decomposition-based architectures for physics-informed neural networks*, SAM Research Report, (2023).
- [17] V. DOLEAN, A. HEINLEIN, S. MISHRA, AND B. MOSELEY, *Finite basis physics-informed neural networks as a Schwarz domain decomposition method*, in Domain Decomposition Methods in Science and Engineering XXVII, Springer Nature Switzerland, 2024, pp. 165–172.
- [18] V. DOLEAN, P. JOLIVET, AND F. NATAF, *An introduction to domain decomposition methods: algorithms, theory, and parallel implementation*, SIAM Philadelphia, 2015.
- [19] M. DRYJA, *An additive Schwarz algorithm for two- and three-dimensional finite element elliptic problems*, in Domain Decomposition Methods, SIAM Philadelphia, 1989, pp. 168–172.
- [20] M. DRYJA AND O. B. WIDLUND, *Towards a unified theory of domain decomposition algorithms for elliptic problems*, in Third International Symposium on Domain Decomposition Methods for Partial Differential Equations, SIAM Philadelphia, 1990, pp. 3–21.
- [21] L. GAEDKE-MERZHÄUSER, A. KOPANIČÁKOVÁ, AND R. KRAUSE, *Multilevel minimization for deep residual networks*, ESAIM: Proceedings and Surveys, 71 (2021), pp. 131–144.
- [22] X. GLOROT AND Y. BENGIO, *Understanding the difficulty of training deep feedforward neural networks*, in Proceedings of the Thirteenth International Conference on Artificial Intelligence and Statistics, vol. 9, PMLR, 2010, pp. 249–256.
- [23] S. GRATTON, A. KOPANIČÁKOVÁ, AND P. L. TOINT, *Multilevel objective-function-free optimization with an application to neural networks training*, SIAM Journal on Optimization, 33 (2023), pp. 2772–2800.
- [24] C. GREIF, T. REES, AND D. B. SZYLD, *GMRES with multiple preconditioners*, SeMA Journal, 74 (2017), pp. 213–231.
- [25] L. GU, W. ZHANG, J. LIU, AND X.-C. CAI, *Decomposition and composition of deep convolutional neural networks and training acceleration via sub-network transfer learning*, Elec-

- tronic Transactions on Numerical Analysis, (2022), pp. 157–186.
- [26] S. GÜNTHER, L. RUTHOTTO, J. B. SCHRODER, E. C. CYR, AND N. R. GAUGER, *Layer-parallel training of deep residual neural networks*, SIAM Journal on Mathematics of Data Science, 2 (2020), pp. 1–23.
- [27] D. A. HAM, P. H. J. KELLY, L. MITCHELL, C. J. COTTER, R. C. KIRBY, K. SAGIYAMA, N. BOUZIANI, S. VORDERWUELBECKE, T. J. GREGORY, J. BETTERIDGE, D. R. SHAPERO, R. W. NIXON-HILL, C. J. WARD, P. E. FARRELL, P. D. BRUBECK, I. MARSDEN, T. H. GIBSON, M. HOMOLYA, T. SUN, A. T. T. MCRAE, F. LUPORINI, A. GREGORY, M. LANGE, S. W. FUNKE, F. RATHGEBER, G.-T. BERCEA, AND G. R. MARKALL, *Firedrake User Manual*, Imperial College London and University of Oxford and Baylor University and University of Washington, first edition ed., 5 2023, <https://doi.org/10.25561/104839>.
- [28] K. HE, X. ZHANG, S. REN, AND J. SUN, *Deep residual learning for image recognition*, in Proceedings of the IEEE Conference on Computer Vision and Pattern Recognition, 2016, pp. 770–778.
- [29] Z. HU, A. D. JAGTAP, G. E. KARNIADAKIS, AND K. KAWAGUCHI, *Augmented physics-informed neural networks (APINNs): A gating network-based soft domain decomposition methodology*, Engineering Applications of Artificial Intelligence, 126 (2023), p. 107183.
- [30] Y. HUANG, Y. CHENG, A. BAPNA, O. FIRAT, D. CHEN, M. CHEN, H. LEE, J. NGIAM, Q. V. LE, Y. WU, ET AL., *GPipe: Efficient training of giant neural networks using pipeline parallelism*, in Advances in Neural Information Processing Systems, vol. 32, 2019, pp. 103–112.
- [31] A. JACOT, F. GABRIEL, AND C. HONGLER, *Neural tangent kernel: Convergence and generalization in neural networks*, in Advances in Neural Information Processing Systems, vol. 31, 2018, pp. 8580–8589.
- [32] A. D. JAGTAP AND G. E. KARNIADAKIS, *Extended physics-informed neural networks (XPINNs): A generalized space-time domain decomposition based deep learning framework for nonlinear partial differential equations*, Communications in Computational Physics, 28 (2020).
- [33] A. D. JAGTAP, K. KAWAGUCHI, AND G. E. KARNIADAKIS, *Adaptive activation functions accelerate convergence in deep and physics-informed neural networks*, Journal of Computational Physics, 404 (2020), p. 109136.
- [34] A. D. JAGTAP, E. KHARAZMI, AND G. E. KARNIADAKIS, *Conservative physics-informed neural networks on discrete domains for conservation laws: Applications to forward and inverse problems*, Computer Methods in Applied Mechanics and Engineering, 365 (2020), p. 113028.
- [35] G. E. KARNIADAKIS, I. G. KEVREKIDIS, L. LU, P. PERDIKARIS, S. WANG, AND L. YANG, *Physics-informed machine learning*, Nature Reviews Physics, 3 (2021), pp. 422–440.
- [36] D. P. KINGMA AND J. BA, *Adam: A method for stochastic optimization*, arXiv preprint arXiv:1412.6980, (2014).
- [37] A. KLAWONN, M. LANSER, AND J. WEBER, *A domain decomposition-based CNN-DNN architecture for model parallel training applied to image recognition problems*, arXiv preprint arXiv:2302.06564, (2023).
- [38] A. KOPANIČÁKOVÁ, *DON dataset: AnisotropicDiffusion2D*, 2024, <https://doi.org/https://doi.org/10.5281/zenodo.10909052>, <https://doi.org/10.5281/zenodo.10909052>.
- [39] A. KOPANIČÁKOVÁ, *DON dataset: NonNestedHelmholtz3D*, 2024, <https://doi.org/https://doi.org/10.5281/zenodo.10904349>, <https://doi.org/10.5281/zenodo.10904349>.
- [40] A. KOPANIČÁKOVÁ, H. KOTHARI, G. E. KARNIADAKIS, AND R. KRAUSE, *Enhancing training of physics-informed neural networks using domain decomposition-based preconditioning strategies*, SIAM Journal on Scientific Computing, (2024), pp. S46–S67.
- [41] A. KOPANIČÁKOVÁ, H. KOTHARI, AND R. KRAUSE, *Nonlinear field-split preconditioners for solving monolithic phase-field models of brittle fracture*, Computer Methods in Applied Mechanics and Engineering, 403 (2023), p. 115733.
- [42] A. KOPANIČÁKOVÁ, Y. LEE, AND H. KOTHARI, *DistTrainNN: Model parallel framework for distributed training of scientific machine-learning applications*. Git repository. [https://bitbucket.org/alena\\_kopanicakova/disttrainn](https://bitbucket.org/alena_kopanicakova/disttrainn), 2023, [https://bitbucket.org/alena\\_kopanicakova/disttrainn](https://bitbucket.org/alena_kopanicakova/disttrainn).
- [43] A. KOPANIČÁKOVÁ AND R. KRAUSE, *Globally convergent multilevel training of deep residual networks*, SIAM Journal on Scientific Computing, (2022), pp. S254–S280.
- [44] H. KOTHARI, A. KOPANIČÁKOVÁ, AND R. KRAUSE, *Nonlinear Schwarz preconditioning for nonlinear optimization problems with bound constraints*, in Domain Decomposition Methods in Science and Engineering XXVII, Springer Nature Switzerland, 2024, pp. 319–326.
- [45] A. KRIZHEVSKY, *One weird trick for parallelizing convolutional neural networks*, arXiv preprint arXiv:1404.5997, (2014).

- [46] F. KUNSTNER, V. SANCHES PORTELLA, M. SCHMIDT, AND N. HARVEY, *Searching for optimal per-coordinate step-sizes with multidimensional backtracking*, in Advances in Neural Information Processing Systems, vol. 36, 2024, pp. 2725–2767.
- [47] Y. LEE, J. PARK, AND C.-O. LEE, *Parareal neural networks emulating a parallel-in-time algorithm*, IEEE Transactions on Neural Networks and Learning Systems, (2022).
- [48] Y. LEE, J. PARK, AND C.-O. LEE, *Two-level group convolution*, Neural Networks, 154 (2022), pp. 323–332.
- [49] Z. LI, N. B. KOVACHKI, K. AZIZZADENESHELI, B. LIU, K. BHATTACHARYA, A. STUART, AND A. ANANDKUMAR, *Fourier neural operator for parametric partial differential equations*, in International Conference on Learning Representations, 2021.
- [50] P.-L. LIONS ET AL., *On the Schwarz alternating method. I*, in First International Symposium on Domain Decomposition Methods for Partial Differential Equations, vol. 1, Paris, France, 1988, p. 42.
- [51] D. C. LIU AND J. NOCEDAL, *On the limited memory BFGS method for large scale optimization*, Mathematical Programming, 45 (1989), pp. 503–528.
- [52] L. LU, P. JIN, G. PANG, Z. ZHANG, AND G. E. KARNIADAKIS, *Learning nonlinear operators via DeepONet based on the universal approximation theorem of operators*, Nature Machine Intelligence, 3 (2021), pp. 218–229.
- [53] L. LU, X. MENG, S. CAI, Z. MAO, S. GOSWAMI, Z. ZHANG, AND G. E. KARNIADAKIS, *A comprehensive and fair comparison of two neural operators (with practical extensions) based on fair data*, Computer Methods in Applied Mechanics and Engineering, 393 (2022), p. 114778.
- [54] L. LU, R. PESTOURIE, W. YAO, Z. WANG, F. VERDUGO, AND S. G. JOHNSON, *Physics-informed neural networks with hard constraints for inverse design*, SIAM Journal on Scientific Computing, 43 (2021), pp. B1105–B1132.
- [55] L. LUO AND X.-C. CAI, *Preconditioned inexact Newton with learning capability for nonlinear system of equations*, SIAM Journal on Scientific Computing, 45 (2023), pp. A849–A871.
- [56] S. MISHRA AND R. MOLINARO, *Estimates on the generalization error of physics-informed neural networks for approximating a class of inverse problems for PDEs*, IMA Journal of Numerical Analysis, 42 (2022), pp. 981–1022.
- [57] W. J. MOROKOFF AND R. E. CAFLISCH, *Quasi-Monte Carlo integration*, Journal of Computational Physics, 122 (1995), pp. 218–230.
- [58] D. NARAYANAN, A. HARLAP, A. PHANISHAYEE, V. SESHADRI, N. R. DEVANUR, G. R. GANGER, P. B. GIBBONS, AND M. ZAHARIA, *PipeDream: Generalized pipeline parallelism for dnn training*, in ACM Symposium on Operating Systems Principles, 2019, pp. 1–15.
- [59] A. PASZKE, S. GROSS, F. MASSA, A. LERER, J. BRADBURY, G. CHANAN, T. KILLEEN, Z. LIN, N. GIMELSHEIN, L. ANTIGA, A. DESMAISON, A. KÖPF, E. YANG, Z. DEVITO, M. RAISON, A. TEJANI, S. CHILAMKURTHY, B. STEINER, L. FANG, J. BAI, AND S. CHINTALA, *PyTorch: An imperative style, high-performance deep learning library*, in Advances in Neural Information Processing Systems, vol. 32, 2019, pp. 8026–8037.
- [60] M. RAISSI, P. PERDIKARIS, AND G. E. KARNIADAKIS, *Physics-informed neural networks: A deep learning framework for solving forward and inverse problems involving nonlinear partial differential equations*, Journal of Computational Physics, 378 (2019), pp. 686–707.
- [61] M. RUDAKOV, A. BEZDOSIKOV, Y. KHOLODOV, AND A. GASNIKOV, *Activations and gradients compression for model-parallel training*, Doklady Mathematics, 108 (2023), pp. S272–S281.
- [62] J. W. SIEGEL AND J. XU, *Approximation rates for neural networks with general activation functions*, Neural Networks, 128 (2020), pp. 313–321.
- [63] J. SIRIGNANO AND K. SPILIOPOULOS, *DGM: A deep learning algorithm for solving partial differential equations*, Journal of Computational Physics, 375 (2018), pp. 1339–1364.
- [64] N. SUKUMAR AND A. SRIVASTAVA, *Exact imposition of boundary conditions with distance functions in physics-informed deep neural networks*, Computer Methods in Applied Mechanics and Engineering, 389 (2022), p. 114333.
- [65] A. TOSELLI AND O. WIDLUND, *Domain decomposition methods-algorithms and theory*, Springer Berlin, 2004.
- [66] S. WANG, Y. TENG, AND P. PERDIKARIS, *Understanding and mitigating gradient flow pathologies in physics-informed neural networks*, SIAM Journal on Scientific Computing, 43 (2021), pp. A3055–A3081.
- [67] S. WANG, H. WANG, AND P. PERDIKARIS, *Learning the solution operator of parametric partial differential equations with physics-informed DeepONets*, Science Advances, 7 (2021), p. eabi8605.
- [68] S. WANG, X. YU, AND P. PERDIKARIS, *When and why PINNs fail to train: A neural tangent kernel perspective*, Journal of Computational Physics, 449 (2022), p. 110768.